Global dynamics of the offshore wind energy sector monitored with Sentinel-1: Turbine count, installed capacity and site specifications

Thorsten Hoeser[1,*] Claudia Kuenzer[1,2]

[1]German Remote Sensing Data Center (DFD), German Aerospace Center (DLR)
[2]Department of Remote Sensing, Institute of Geography and Geology, University of Wuerzburg

[*]Corresponding author, thorsten.hoeser@dlr.de

Statement: This is a non-peer reviewed preprint submitted to EarthArXiv. This manuscript has been submitted to the International Journal of Applied Earth Observation and Geoinformation to be considered for publication. Future versions may have different content based on the peer review process.

Global dynamics of the offshore wind energy sector monitored with Sentinel-1: Turbine count, installed capacity and site specifications

Preprint, submitted 20. Apr. 2022

Thorsten Hoeser[1,*] Claudia Kuenzer[1,2]

[1]German Remote Sensing Data Center (DFD), German Aerospace Center (DLR)
[2]Department of Remote Sensing, Institute of Geography and Geology, University of Wuerzburg

[*]Corresponding author, thorsten.hoeser@dlr.de

Abstract

With the promotion of renewable energy production and a planned phaseout of fossil fuels until 2040, the offshore wind energy sector has started to expand and will continue to increase its capacity in the upcoming decades. This study presents how the installed capacity can be derived from radar imagery provided by the Sentinel-1 mission for all offshore wind turbines on the entire Earth. By further combining freely available Earth observation and GIS data, commonly reported attributes of the offshore wind energy sector are compiled. All attributes are investigated to provide an in-depth overview of the developments of the offshore wind energy sector over the last five years. Between 2016 and 2021, the installed capacity worldwide grew from 13.5 GW to 40.6 GW. This corresponds to an increase of 27.1 GW or 200%. In total 8,885 offshore wind turbines (OWTs) were installed until June 2021 with an additional 852 under construction. The European Union (15.2 GW), China (14.1 GW) and the United Kingdom (10.7 GW) are the three major contributors to the offshore wind energy sector. China has seen the largest growth in the last five years of 13 GW, followed by the EU with 8 GW and the UK with 5.8 GW. The provided in-depth analysis at the end of this study describes the offshore wind energy sector to be in a transition phase between decades of maturity and massive growth at a time when carbon-neutral energy production is massively supported. Overall the proposed methods for independent offshore wind turbine capacity estimation and spatiotemporal investigation of the offshore wind energy sector can be used by all stakeholders involved in the upcoming challenge of integrated planning and implementation of offshore wind energy projects.

1. Introduction

In the Climate Pact of the 26th UN Climate Change Conference (COP26) in 2021, 65 countries agreed to massively decrease the use of fossil fuels for energy production with a coal phaseout until 2040 [3]. Another agreement urges the transition to zero-emission vehicles, pointing out the necessity of rapid progress in charging infrastructure and enabling the electrical grid for the increasing demand for electric vehicles [4]. These two goals are exemplary for a long-term carbon-neutral society: Energy production based on fossil fuels has to phase out while the demand for electrical power by new, carbon-neutral technologies increases. Electrical power generation has to change and expand simultaneously to achieve both goals. Therefore, a major contribution to future energy production in carbon-neutral societies will be a massive increase in renewable energy.

The offshore wind energy sector has grown steadily since 1991 and has become an important contributor to a carbon-neutral energy mix [22]. With the current promotion of renewable energy, there will be a massive expansion in the upcoming decades. In 2021, the UK government introduced the Net Zero Strategy, which targets to increase its offshore wind energy capacity from 10.5 GW in 2020 to 40 GW by 2030 [27]. With an investment of EUR 800 billion, the EU announced expanding its offshore wind energy capacity from 12 GW in 2020 to 60 GW in 2030 and up to 300 GW in 2050 [6]. These two strategies will mainly affect the North Sea Basin. However, with an already ongoing and worldwide most extensive expansion in China and recently started constructions in the United States, the South and East China Sea and the US Atlantic coast are further examples that demonstrate the global scale of the offshore wind energy expansion [22]. Thus, offshore wind energy in-

frastructure deployment in marine space will increase dramatically. Today, many stakeholders are involved, and legal, economic, and ecological conflicts have to be considered along with the urgent task of deploying carbon-neutral energy infrastructure [10]. Therefore, public access to independent information and ongoing monitoring of the development of the offshore wind energy sector is crucial.

Recent developments in image processing, especially from the deep learning domain [14, 18, 31], and free access to remote sensing data enable users to extract small scale single object entities in large-scale Earth observation archives [12]. Recently, Hoeser et al. [13] introduced the DeepOWT data set, a global data set of offshore wind energy infrastructure which provides single offshore wind turbine (OWT) locations along with their deployment stages between 2016 and 2021, based on Earth observation data. In this study, the DeepOWT data set is employed to model the installed capacity of offshore wind turbines on a local to global scale and conduct an in-depth investigation of key attributes of the offshore wind energy sector over the last five years. Therefore, new data, which highly increases the information depth of the spatiotemporal DeepOWT data set, is derived from freely available Earth observation data. Thus, this application of Earth observation and geoinformation is an example of how data and techniques from these domains can be used to investigate the current developments in the offshore wind energy sector.

2. Related Research

Studies of detecting persistent marine infrastructure with Earth observation data have been carried out to provide data that can be used to investigate the human impact on marine ecosystems or to report the development of specific industries like oil production or offshore renewable energy. Radar remote sensing is specifically suitable since it is unaffected by clouds and offshore objects appear as bright backscatter clusters in front of the darker sea with a low backscatter coefficient. These imaging characteristics are commonly used to investigate offshore infrastructure. Wong et al. [28] proposed a detection process based on the constant false alarm rate (CFAR) approach, which investigates preprocessed Sentinel-1 images by the difference of Gaussians (DoG) method to find object locations and further postprocessing to weed out false positives. They deployed their algorithm on the Google Earth Engine and detected oil rigs in the Gulf of Mexico and offshore wind turbines in the exclusive economic zones of the UK and China. Zhang et al. [30] processed the Sentinel-1 archive on a global scale and provided OWT locations by applying a morphological approach in combination with multiple thresholds to remove false positives. In addition to the spatial locations, the estimated first appearance of an OWT between 2014 and 2019 is provided in their study. Xu et al. [29] investigated multispectral images from the Sentinel-2 and Landsat missions. They used order statistic filtering in combinations with predefined thresholds to extract marine infrastructure. By combining the object candidates with existing vector geometries of offshore wind farms or human interpretation, they were able to distinguish only offshore wind energy infrastructure further.

In a proceeding study to this work, Hoeser et al. [13] proposed the DeepOWT data set, which provides offshore wind energy infrastructure objects along with their deployment dynamics. Figure 1 summarises how the DeepOWT data set was derived from Sentinel-1 images on a global scale. Thereby, Sentinel-1 acquisitions of the second quarter of 2021 were reduced to median composites on which a cascade of two convolutional neural networks (CNN), optimised on fully synthetic training data [15], detect offshore wind energy infrastructure. OWTs, transformer stations and platforms under construction were differentiated during the detection of the second CNN. Based on the detected bounding box of an object, the multi-temporal deployment dynamics were derived by investigating changes in the local radar signature for a five year stack of quarterly images. The final DeepOWT data set provides point locations that describe offshore wind energy infrastructure and their quarterly deployment stages from July 2016 until June 2021.

The reported studies mainly focus on improving spatiotemporal information. However, an important metric besides the location and deployment stage of an OWT is the installed capacity. As reported in section 1, this metric is commonly used to inform about the size and development of the offshore wind energy sector and to communicate expansion goals of offshore wind energy strategies for the upcoming decades. Therefore, this study uses the spatiotemporal information provided by the DeepOWT data set to model this essential metric on a global scale based on Earth observation data.

3. Data and Material

This study uses the recently published DeepOWT data set due to its open accessibility, accurate spatiotemporal information and underlying Earth observation data, the Sentinel-1 archive. DeepOWT describes turbine locations with a quarterly time series from July 2016 until June 2021 along with the information if a turbine is under construction, readily deployed, or neither of both [13]. Figure 2 gives an impression of the data set, its global extent, two regional hot spots and a local example of turbine and transformer station locations for a large OWT cluster in the North Sea Basin. To further enrich the information for each single OWT location, the Google Earth Engine (GEE) [9] was used to query Sentinel-1 C-band radar data [26] for calculating the OWT height and installed capacity. Ground truth data of 50 OWT clusters regarding their hub height and the cor-

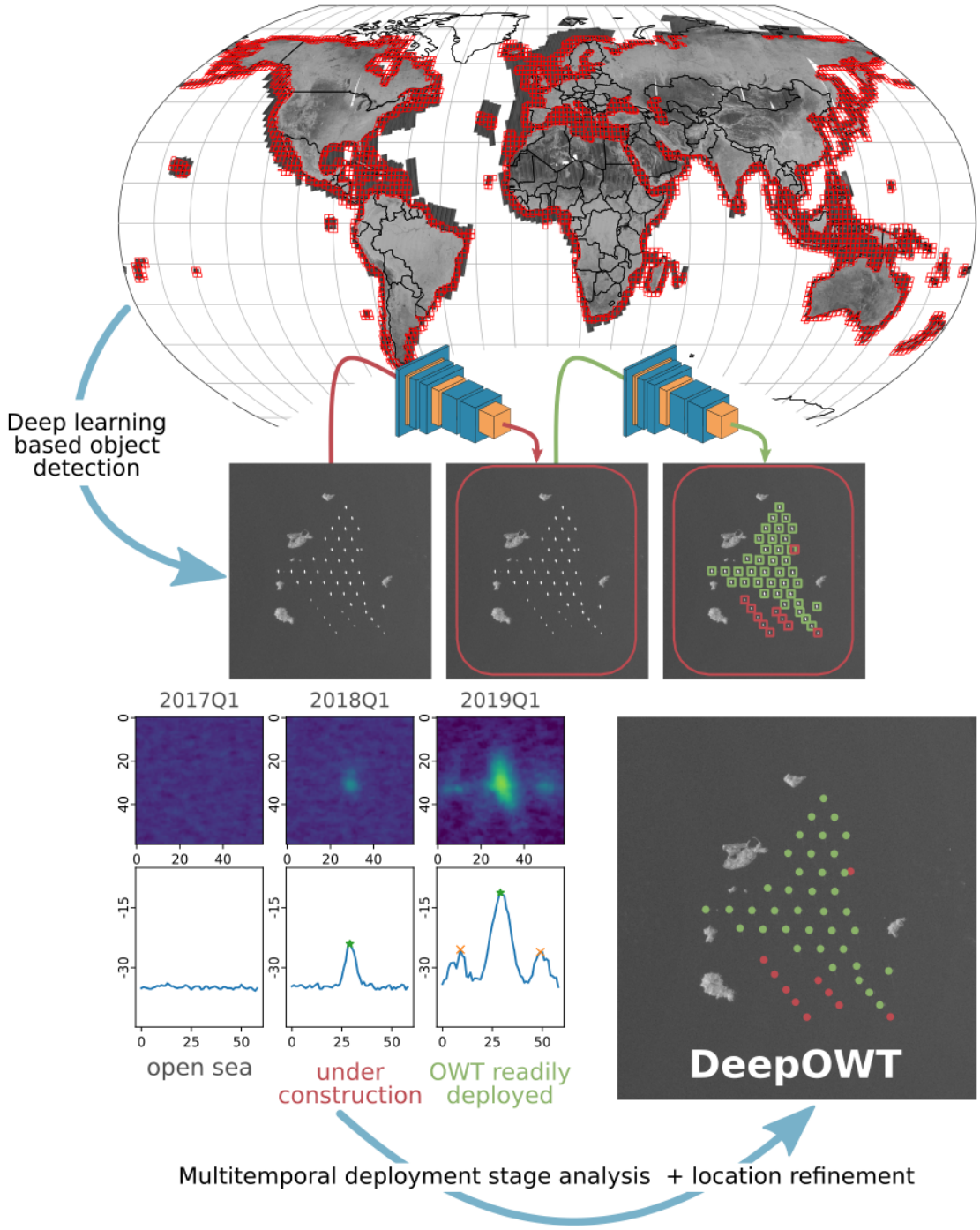

Figure 1. Graphical summary of the workflow which has been used to derive the DeepOWT data set by Hoeser et al. [13]. Two convolutional neural networks analyse global Sentinel-1 data to find OWT locations. A time series from July 2016 until June 2021 is analysed for each OWT location to derive its deployment dynamics.

responding capacity in MW were acquired from publicly available sources, like OWF operator specifications or public planning documents. This data was used to validate the height calculation based on the Sentinel-1 images and to build the statistical model which links OWT height to OWT installed capacity. Moreover, the water depth from NOAA's ETOPO1 topography data set, available on the GEE, was also queried for each turbine location [1]. Furthermore, the

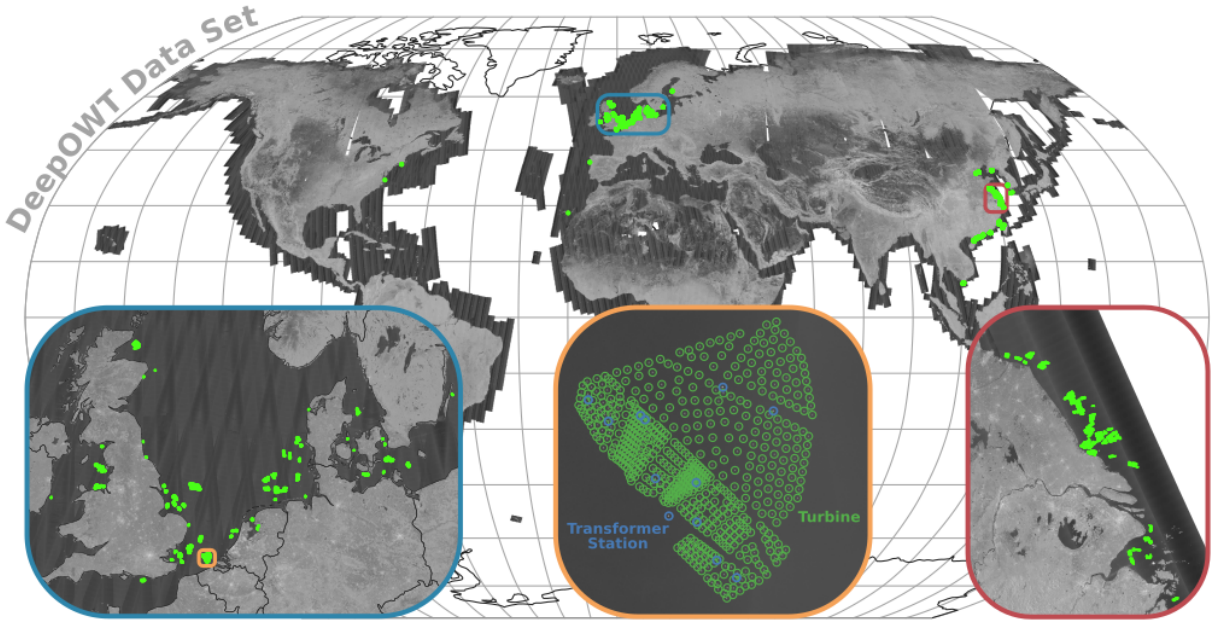

Figure 2. Locations of offshore wind energy infrastructure provided in the DeepOWT data set. The magnifications show OWT clusters in the North Sea basin, a local close up of one large OWT cluster of the Netherlands and Belgium and OWT clusters in the northern East China Sea in June 2021.

OWT locations from DeepOWT are combined with vector data which describe the exclusive economic zones (EEZ) [8] and the global coastline [20] to derive national affiliation and the minimum distance to the coast for each OWT, respectively.

4. Methodology

4.1. Installed capacity estimation

In order to design an independent and region agnostic estimation of the installed capacity, the workflow was based on freely and globally available Sentinel-1 data. Two steps were used to derive the installed capacity of an OWT from spaceborne radar imagery. In step one, the turbine's hub height is calculated by a radargrammetric investigation of the radar signature at an OWT location. In step two, a model links the calculated hub height to the installed capacity for each turbine.

4.1.1 Offshore wind turbine height calculation

Figure 3a) shows conceptually how the hub height of an OWT was calculated with Sentinel-1 data. A rectangular 400×400 m area was defined for each OWT location. For these areas, all Sentinel-1 acquisitions between April to June 2021 with the specification GRD (ground range detected), IW (interferometric wide swath), VH (vertical horizontal polarised), ascending orbit and from a single platform A or B were stacked and reduced to a single band median image. The example in figure 3 shows two main backscatter clusters. One large cluster in the centre at the detected location of an OWT and left to it, a smaller cluster. The smaller cluster to the left of the OWT appears due to the right looking sensor geometry, and the layover effect [19] depicted in 3b). The radar signal first hits the nacelle before hitting the larger foundation at sea level. Thus, when projected onto the ground range, the part of the signal that hits the nacelle gets distorted and appears in front of the undistorted centre location. Visually in map-view, it looks like the turbine leans over towards the sensor.

Furthermore, 3c) and d) describe how the resulting geometry can be used for height calculation. 3c) describes how the local incident angle θ increases with increasing ground range. At the same time, α increases too, allowing to approximate a right angle between the theoretical hypotenuse of nacelle and layover cluster, and the radar signal with a local incident angle θ_{OWT} at the OWT location, see figure 3d). It follows that α and θ_{OWT} are equal.

A theoretical right triangle can be constructed to calculate the hub height of the OWT, where the side opposite is the hub height, the side adjacent is the absolute distance between the centre cluster and layover cluster and α its corresponding angle. The layover cluster location was extracted by applying a peak finder algorithm on the maximum swath profile along the horizontal axis of the radar image, see 3e). By reprojecting the coordinates of OWT and layover centre to their corresponding UTM coordinate system, the abso-

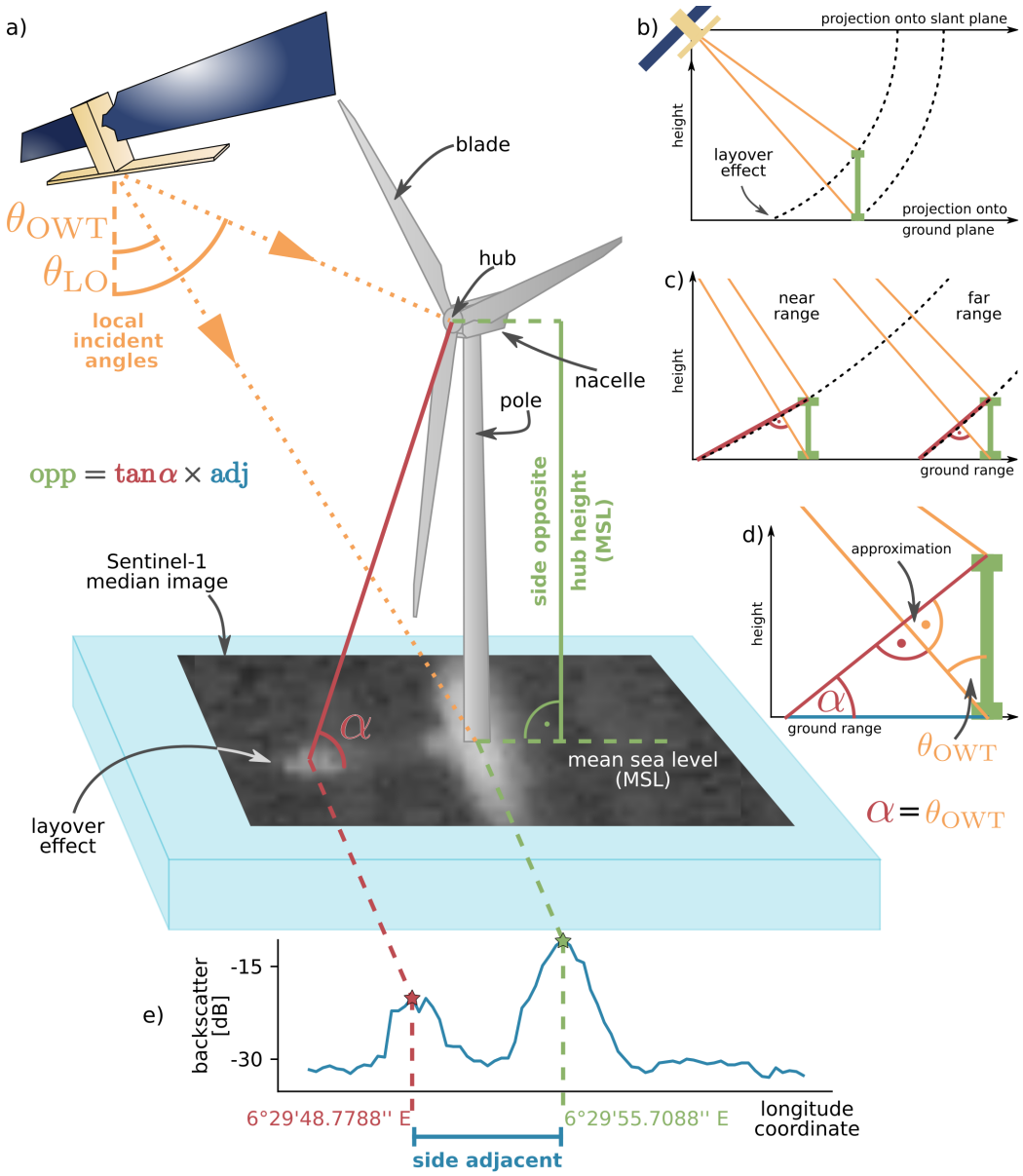

Figure 3. Conceptual visualistion of hub height calculation of an offshore wind turbine by investigating the layover effect and imageing geometry of the Sentinel-1 radar signal.

lute distance between the points was calculated. The calculation of the side opposite was done cluster wise for each OWT. Hereby, an OWT cluster was defined manually by its spatial proximity and OWT deployment date, provided by the DeepOWT data set. In order to reduce outliers of calculated height values, the median of all calculated heights within one cluster defines the final height for all OWTs of the same cluster.

For 50 OWT clusters, the calculated heights were compared to ground truth data. Figure 4 shows that the variance of the calculated heights can explain 77% of the variance of the ground truth heights, and the mean absolute error is 6.45 m. Since the derived locations of OWT and double bounce cluster are the pixel centres in the Sentinel-1 image with a spatial resolution of 10 × 10 m, the side adjacent has a theoretical error ε_{adj} with a range between -10 and +10 m, see figure 5. The maximal contribution of this sub-pixel error to the absolute height error $\varepsilon h_{\varepsilon_{adj}}$ ranges from 6 m to 10.36 m depending on the local incident angle. For Sentinel-1 IW GRD products, the near range angle is θ_{min} (31°), and the far range angle is θ_{max} (46°) [26]. Thus the mean absolute error of 6.45 m of the calculated

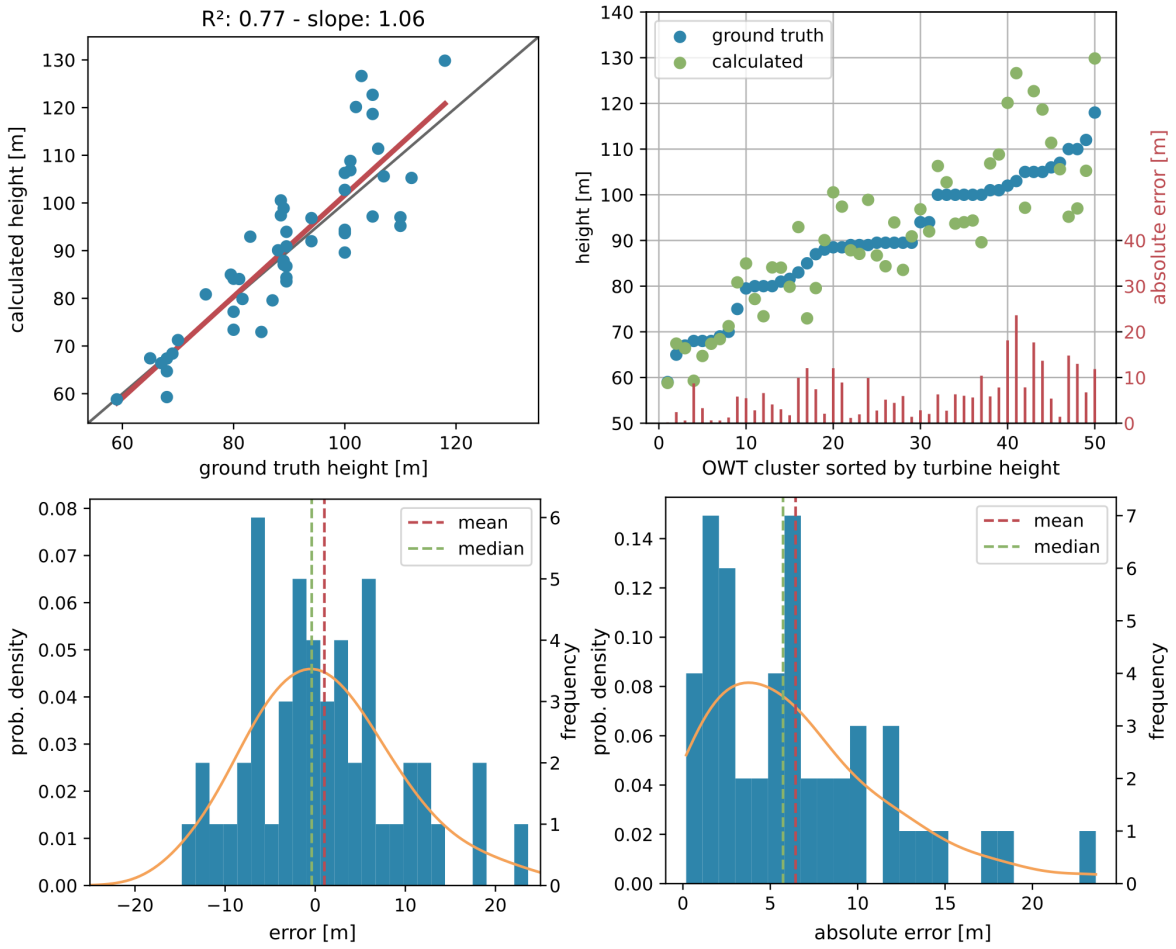

Figure 4. Error discussion of the calculated offshore wind turbine hub heights. The upper row shows the correlation between predicted and ground truth heights and the residuals. The lower row shows the distributions of the error and absolute error.

heights is within the range of the maximum error $\varepsilon h_{\varepsilon_{adj}}$ demonstrating the general practicality of the height calculation approach.

4.1.2 Installed capacity model

In order to model the OWT installed capacity, the data set of 50 OWT clusters for which hub height and nominal capacity were looked up in operator specifications and official planning documents was randomly split into a train and test data set with 36 and 14 entries, respectively. Figure 6 proposes a correlation between hub height and installed capacity of a wind turbine for the train split. With this observation, the parameter *installed capacity* can be estimated by using the calculated height as the independent variable. The hypothetical model h is a sigmoid function, see equation 1, in order to approximate logistic growth where L is the curve's maximum, k the logistic growth rate, x_0 the offset of the x-axis and b the offset of the y-axis.

$$h(x) = \frac{L}{1 + e^{-k(x - x_0)}} + b \tag{1}$$

The sigmoid model hypothesis allows approximating the logistic growth, which can be recognised in the first half of the training data between hub heights of 60 to about 95 m. However, the further progression beyond 95 m diverges from a purely logistic growth, with a higher variance and tendency to level off. Thus the second part of the sigmoid function supports modelling this part of the training data without overestimating higher heights.

The parameters of the hypothetical model are optimised by minimising the least-squares cost function on the train data, resulting in the fitted model shown in figure 6 and its corresponding 95% confidence interval (CI). The optimised model was used to predict the installed capacity for each OWT based on the calculated heights. The predictions were compared to the test and also the train ground truth OWT clusters. The corresponding error distribution of test

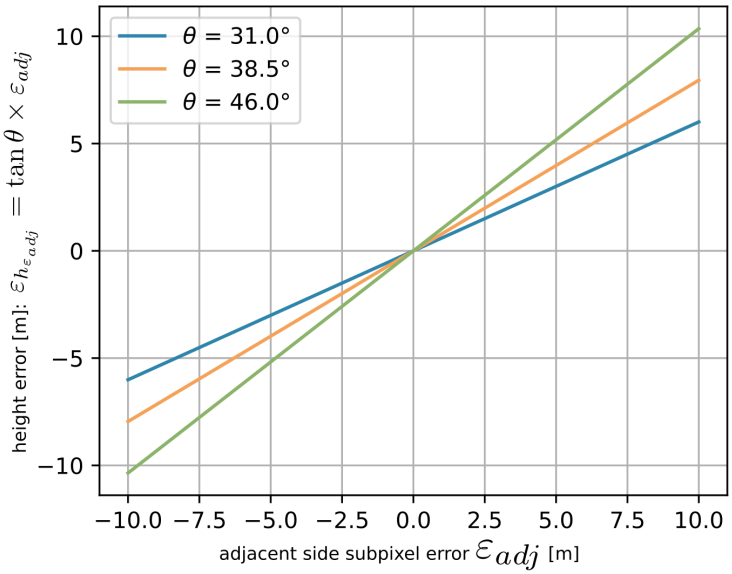

Figure 5. Boundaries of the theoretical contribution to the hub height error caused by location inaccuracy due to the spatial resolution of 10 m and incident angle of the Sentinel-1 sensor. Thereby, the near range incident angle is 31° and the far range incident angle is 46°.

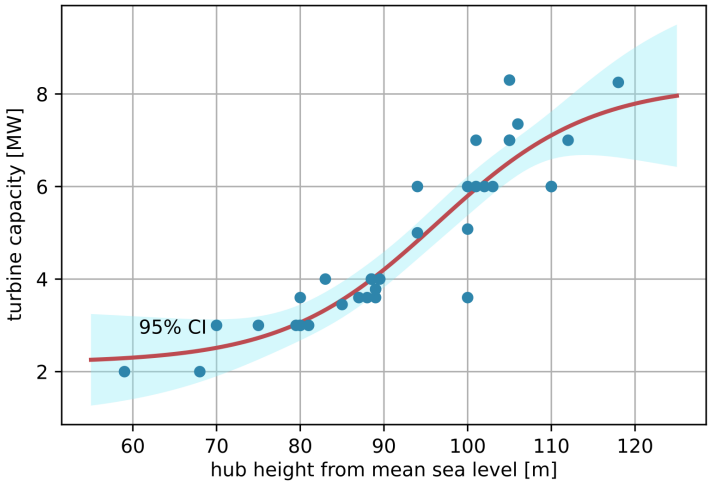

Figure 6. Training data and fitted sigmoid function with its corresponding 95% confidence interval (CI) to map an offshore wind turbine's hub height to its installed capacity.

and train split were compared by a Kolmogorov-Smirnov (KS) test [23] with a significance level of 0.05. The KS test confirmed the null hypothesis with $p = 0.09$, that both distributions are identical, see figure 7. Thus, in the following error discussion, train and test split are combined.

Figure 7 shows that the variance of the estimated installed capacity can explain 90% of the variance of the ground truth capacity. Furthermore, the error follows a normal distribution with a mean at 4.76 MW close to 0. Thus, no systematical error, which tends to always over or underestimate the installed capacity, was observed. The mean absolute error is 36.16 MW which is less than 15% of the mean installed capacity of the ground truth data of 244.98 MW. For a large scale comparison of the model predictions on more than the 50 OWT clusters, we refer to section 5, where region-based capacities from different sources are compared with the installed capacity estimations in this study.

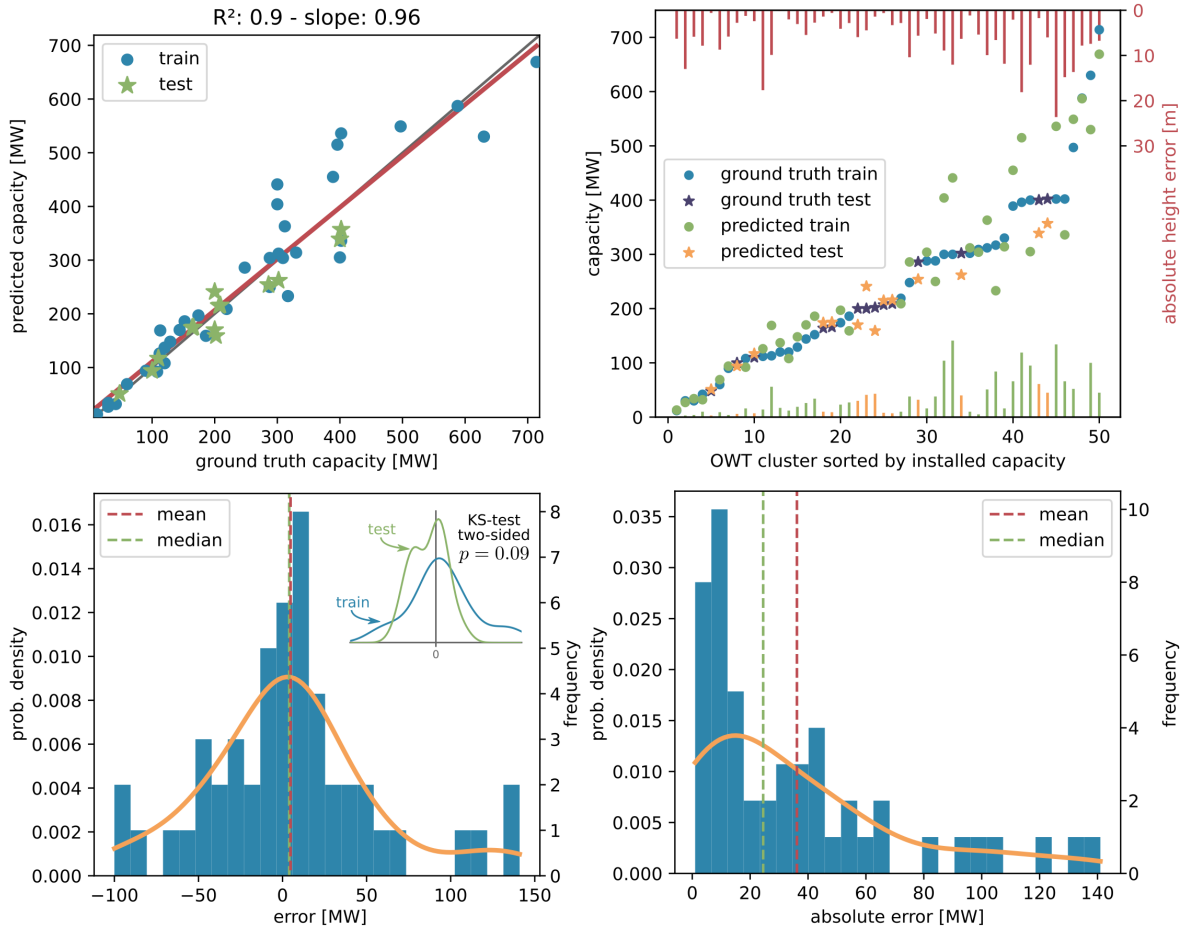

Figure 7. Error discussion of the estimated offshore wind turbine installed capacity. The upper row shows the correlation between predicted and ground truth installed capacity and the residuals. The lower row shows the distributions of the error and absolute error.

4.2. Deriving commonly reported attributes

To further enrich an OWT location besides its hub height and installed capacity, more attributes that are commonly reported in the wind energy sector to describe an offshore wind farm or turbine were derived by spatial queries and geoprocessing.

4.2.1 Offshore wind turbine distance to coast and nearest neighbour

The two characteristics, distance to the nearest OWT and minimum distance to shoreline, were added for each OWT. Every data set used in these processes was reprojected to each OWT location's corresponding UTM coordinate reference system (CRS) before a distance was calculated. No auxiliary data was necessary to calculate the minimum distance between OWTs. Figure 8 shows a pattern of the resulting distances in a European offshore wind farm cluster. This visualisation shows a trend of increasing turbine distance over time due to the installation of OWT with larger rotor diameters.

For the OWT to shoreline distance, the two data sets *Land* and *Minor Islands* from Natural Earth Data [20] of type *large scale 1:10 m* were combined and used as target polygon. In order to minimise the processing effort, for each OWT location, the global data set was clipped with a 200 km radius around the OWT location before searching for the smallest OWT to shoreline distance. Similar to the nearest OWT distance, the distance to the shoreline increases over time for the local example of the east England coast, shown in figure 9. The Hornsea Project, which is also visualised in this figure, is the furthest offshore wind farm project from the mainland, which was partly deployed in 2021.

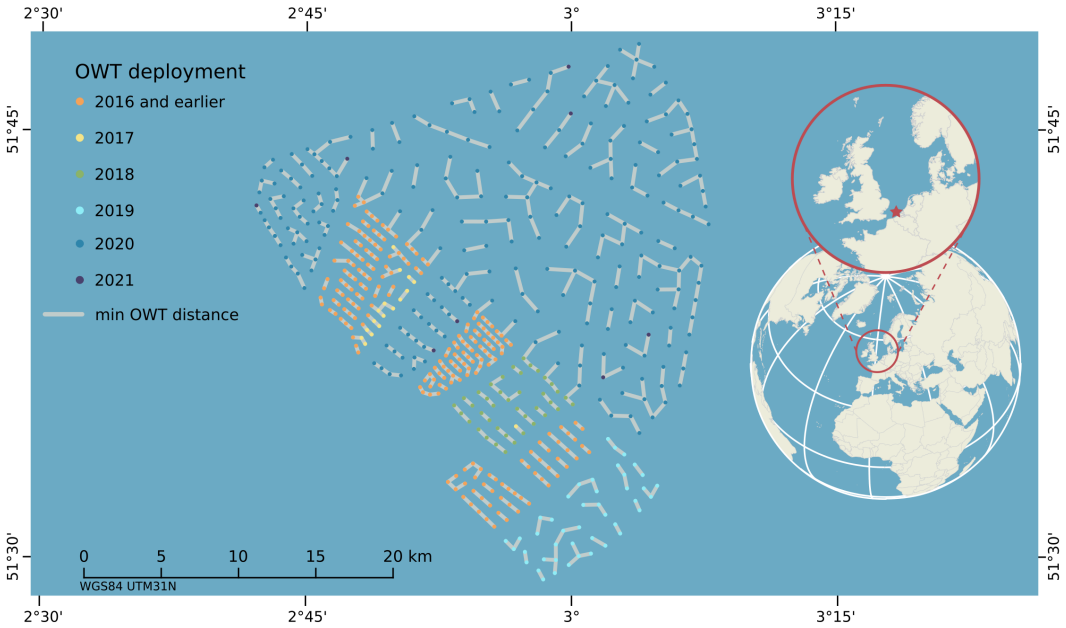

Figure 8. An Offshore wind farm (OWF) cluster in the exclusive economic zones of the Netherlands and Belgium. The temporal dynamic indicates a trend of an increasing distance between single turbines.

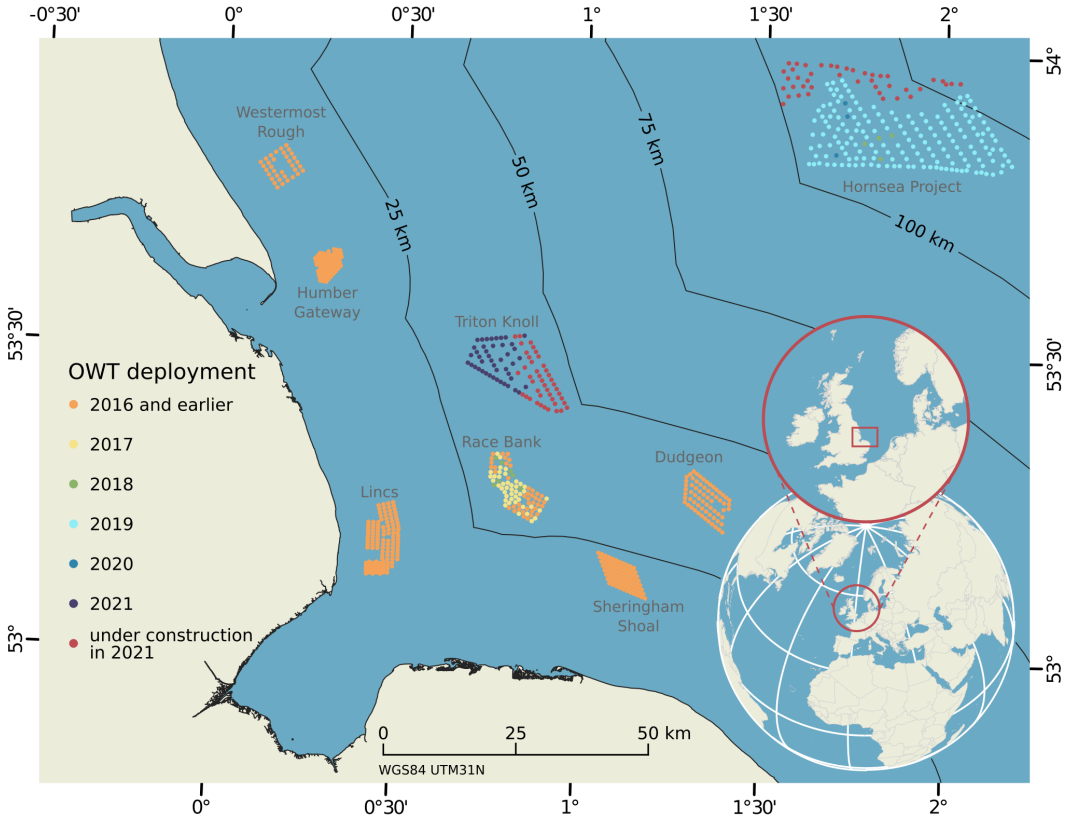

Figure 9. Offshore wind farms (OWF) and their single turbine locations at the East England coast in the North Sea Basin. The temporal dynamic indicates an increasing distance of OWF projects and the shoreline.

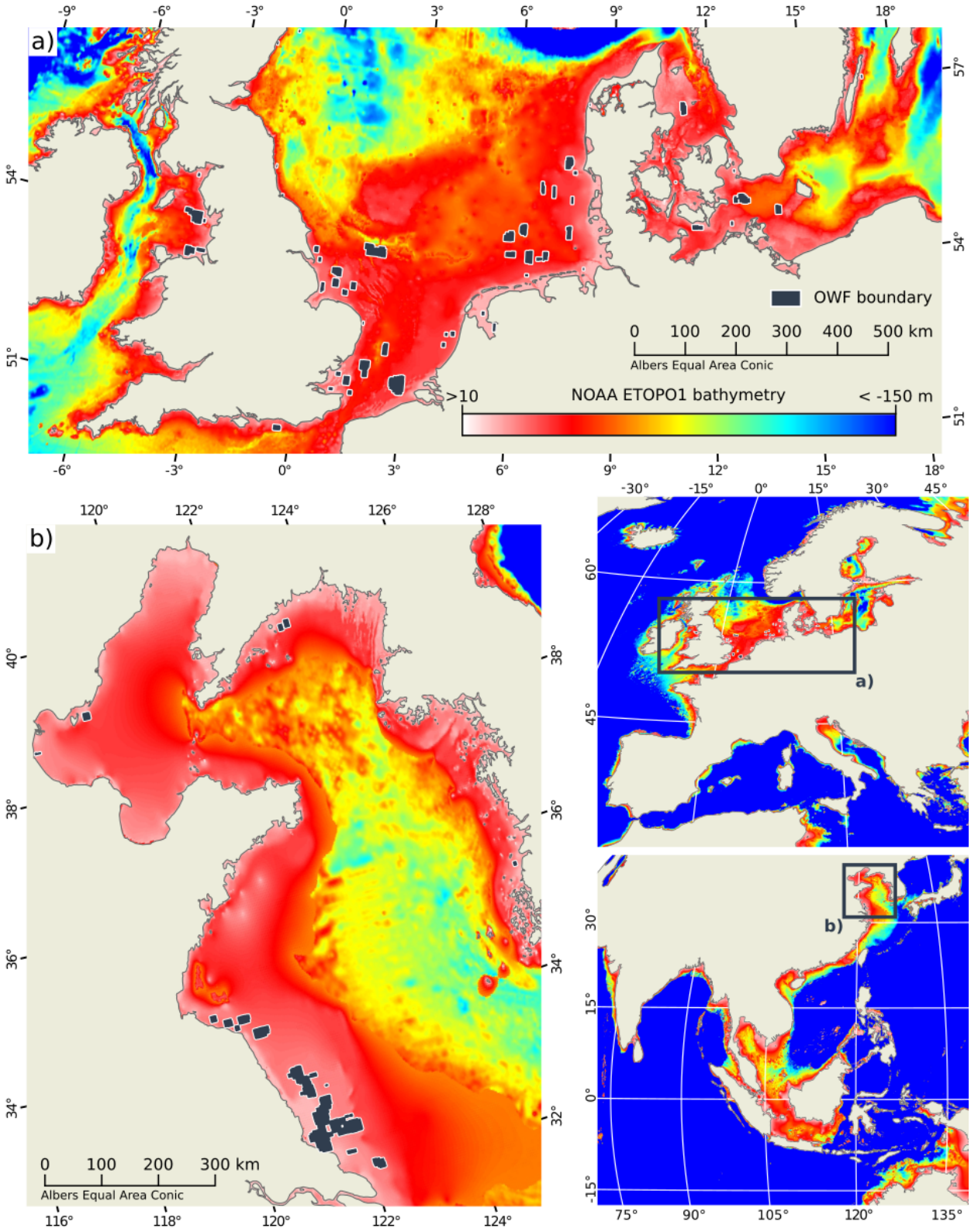

Figure 10. Bathymetry of a) the North Sea Basin and Baltic Sea and b) the northern East China Sea and the Yellow Sea. Both sites show large areas of shallow water depth of about 50 m or less near the coast, which is an important factor for offshore wind farm deployment.

4.2.2 Offshore wind turbine water depth and national affiliation

For the last two attributes, the water depth at an OWT location and the national affiliation, spatial queries are used to obtain the information. In order to get the water depth from a single data source NOAA's ETOPO1 data set [1], which is accessible on the GEE was queried. ETOPO1 describes land topography and ocean bathymetry at a resolution of 1 arc minute on a global scale by combining multiple regional data sets. Figure 10 shows the bathymetry component of the data set for the two wind energy production hotspots, the North Sea Basin; and the northern East China Sea and the Yellow Sea. Both sites show large areas with relatively shallow waters close to the coast, which is one crucial factor for cost-efficient offshore wind turbine deployment. For the European Union, the difference in areas with a shallow water depth of the North Sea Basin compared to the Atlantic ocean and large parts of the Mediterranean is striking, and one explanation why nearly all OWF of the EU are installed in the North Sea Basin and Baltic Sea.

The national affiliation was queried by applying a spatial join with the DeepOWT data set and the national exclusive economic zone (EEZ) layer, the latter provided by the Flanders Marine Institute [8]. This completes the information enrichment of the DeepOWT data set. Six commonly used attributes for the description of offshore wind farm projects [22] have been added to the DeepOWT data set by combining methods from Earth observation, geoinformation and statistics.

5. Results

By combining the DeepOWT data set with further investigations of Sentinel-1 data it was possible to provide installed wind energy capacity estimations based on this single Earth observation mission. In June 2021, the cumulative installed capacity of 8,885 offshore wind turbines was 40.6 GW for the entire Earth. This corresponds to an increase of 27.2 GW or 200% realised by 5,268 OWTs deployed within five years. Figure 11 shows that mainly three big players dominate the offshore wind sector: The European Union, the People's Republic of China and the United Kingdom sorted by installed capacity. Despite one of the worldwide largest onshore wind capacities in the United States of America, offshore wind energy is early with pilot projects and only seven installed OWTs. However, recently construction work has started for large scale offshore wind farms at the Atlantic coast, and new sites are under development in this region.

Figure 11 already suggests recently high deployment dynamics in China with the most wind turbines built and under construction worldwide, which is confirmed in figure 12. In the last five years, China has had the highest increase in both installed capacity and the number of installed OWTs. Figure 13 provides in-depth insight into the temporal deployment dynamics from July 2016 until June 2021. For China, it shows that the onset of offshore wind turbine deployment took place about five years ago and that within the last five years, the global trend of the offshore wind energy sector was greatly influenced by the deployment of 2,960 OWTs with a cumulative capacity of 13 GW. By finishing the planned projects with 627 OWTs under construction in June 2021, in 2022 China will lead in the number of readily deployed OWTs and installed offshore wind turbine capacity worldwide. In comparison, the EU and UK already had numerous offshore wind farms back in 2016, originating from the initial Danish offshore wind farm project Vindeby in 1991 with 5.5 MW and developed the offshore wind sector to maturity over the last decades [22]. Since 2016, the number of OWTs and installed capacity increased by 1,313 OWT and 8 GW, and 916 OWT and 5.8 GW for the EU and UK, respectively. In the upcoming decades, EU's [6] and UK's [27] offshore wind programs will lead to a surge of offshore wind farm projects. Together with China's recent and ongoing contribution, the start of construction work of large-scale offshore wind farms in the US and other nations joining the offshore wind energy sector, these developments will further contribute toward a carbon-neutral energy production on a global scale.

The reported number of installed capacity in this study solely relies on investigations of Earth observation data, as presented in section 4.1. The figures 14 and 15 provide a comparison of the estimated installed capacity results with official reports. The estimated installed capacity of this study is largely confirmed by these reports and can even provide consistently annual numbers. This demonstrates that freely available Earth observation data, in combination with the proposed analysis techniques are able to independently monitor the global dynamics of the offshore wind energy sector. Furthermore, the small-scale resolution based on individual turbines allows a fast and individual aggregation of units in space and time in order to examine developments in detail. This is not possible by using the public reports mentioned above since they only provide aggregated information. The following analysis of the attributes compiled in this study gives an impression of how trends in the offshore wind energy sector can be analysed by flexibly aggregating information in time and space.

Figure 16 provides an overview of temporal dynamics on a global scale and differences between the major offshore wind energy-producing regions for all investigated attributes. Installed capacity and hub height show similar trends and regional characteristics for the same investigation units. The provided quantile regression trend lines show that fewer small OWT units of nominal capacity and hub height were installed over the last five years. Never-

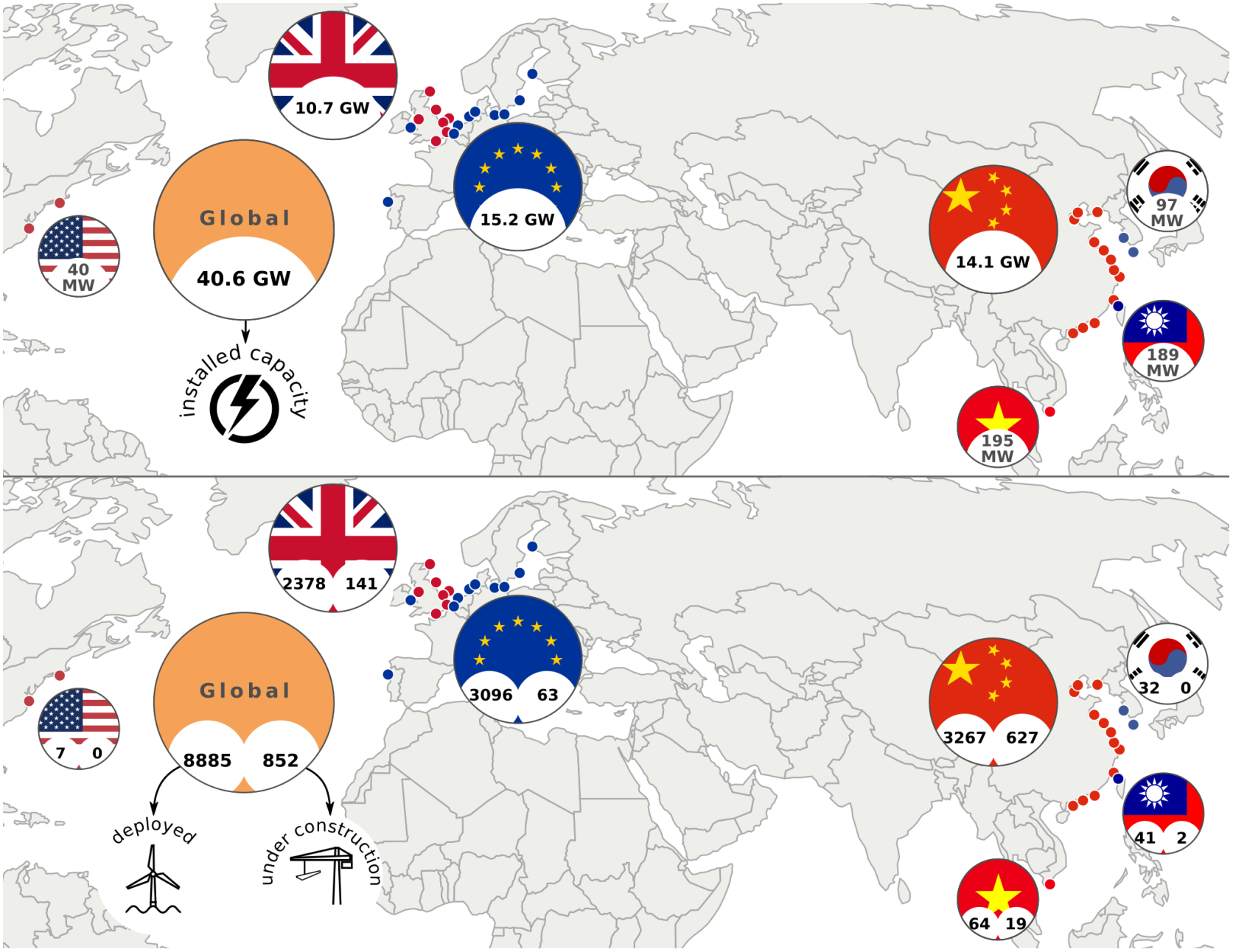

Figure 11. Global distribution of offshore cumulative installed capacity (upper part), and number of offshore wind turbines, readily deployed and under construction (lower part) in the end of June 2021. Single points in the maps indicate clusters of offshore wind farm projects.

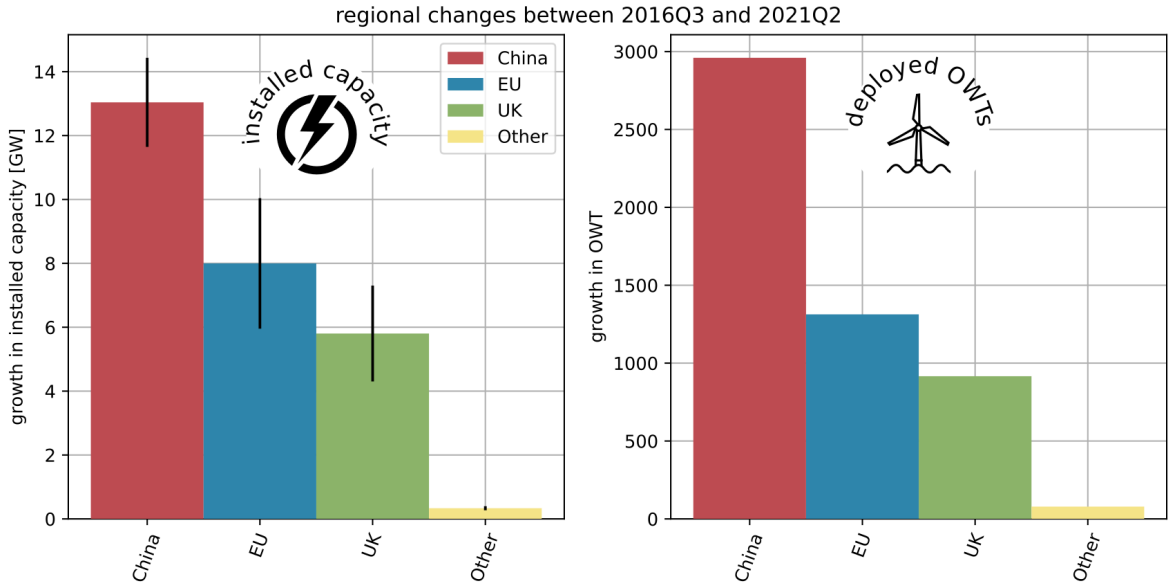

Figure 12. Absolute changes in installed capacity (left) and the number of readily deployed offshore wind turbines (OWT) (right) within five years from July 2016 to June 2021, aggregated by region. The error bars for installed capacity indicate the standard deviation of the model used for the estimation.

theless, at the same time, the trend for larger OWT units is not that clear yet. When looking at regional comparisons and keeping the deployment dynamics of the last five years in mind, it becomes clear that the surge of installed OWTs in China was characterised by OWTs with medium hub height and nominal capacity, about 4 MW, compared to such in the EU or UK. This is an explanation for China having more OWT units than the EU, but the EU had still a higher amount of installed capacity in June 2021, see figure 11. Since China's contribution to the temporal dynamics has been the most influential over the last five years, the Chinese signal subdued the trend of larger OWT units on a global scale. However, when looking at the regional comparison, the EU and UK already have started building larger OWTs with higher nominal capacities, a trend that will continue in the future.

The third row of figure 16 shows the development of the minimum distance to the shoreline. The global temporal trend appears to be mixed and less distinct due to regional peculiarities for this attribute. Most of the OWTs in China are built very close to the shoreline, whereas in the EU, and lately, in the UK, OWTs are built further away from the coast, resulting in a mixed global trend. However, for China and the UK, the temporal trends are clear. New OWTs are getting constructed with increasing distance to the coast. For example, in 2019 the first phase of the Hornsea Project was finished 120 km from the North East coast of England, which can clearly be seen even in the global trend in 2019Q2-2019Q4. More projects with increasing distance to the coast are planned in the EEZ of the UK where shallow waters are available far off the coast, like the Dogger Bank, where the Dogger Bank Wind Farm will be realised in the upcoming years with a maximal distance to the shoreline of about 290 km. The necessity of increasing distance to the shoreline indicates that capacities have already been exploited for a specific region near the shore. For the UK and China, this is a continuously progressive process. For the EU, single EEZs of its members are very different in shape and bathymetry. Thus, it appears to be that no general trend exists. Here, it would be interesting to look at a national scale to see how much of its nearshore capacities each EU member already has used and which bathymetry characteristics are prevalent in general.

The nearest neighbour distance between OWTs shows an increase for higher values, indicating that OWT units with larger rotor diameters that need larger distances to the next OWT are getting installed, which was already locally observed in figure 8. However, the large amount of slightly smaller turbines that were built in China leads to a general trend of smaller distances on a global scale. With the deployment of major offshore wind farm projects completed, like the Jiangsu Qidong in 2021, new projects with larger OWT sizes will also reverse this trend in China and eventually globally.

The last attribute, water depth, appears to be stable over the last five years. Until 2021 OWTs are normally bottom-fixed and directly built on structures that are rammed in the sea ground, known as monopile foundations; tripod or

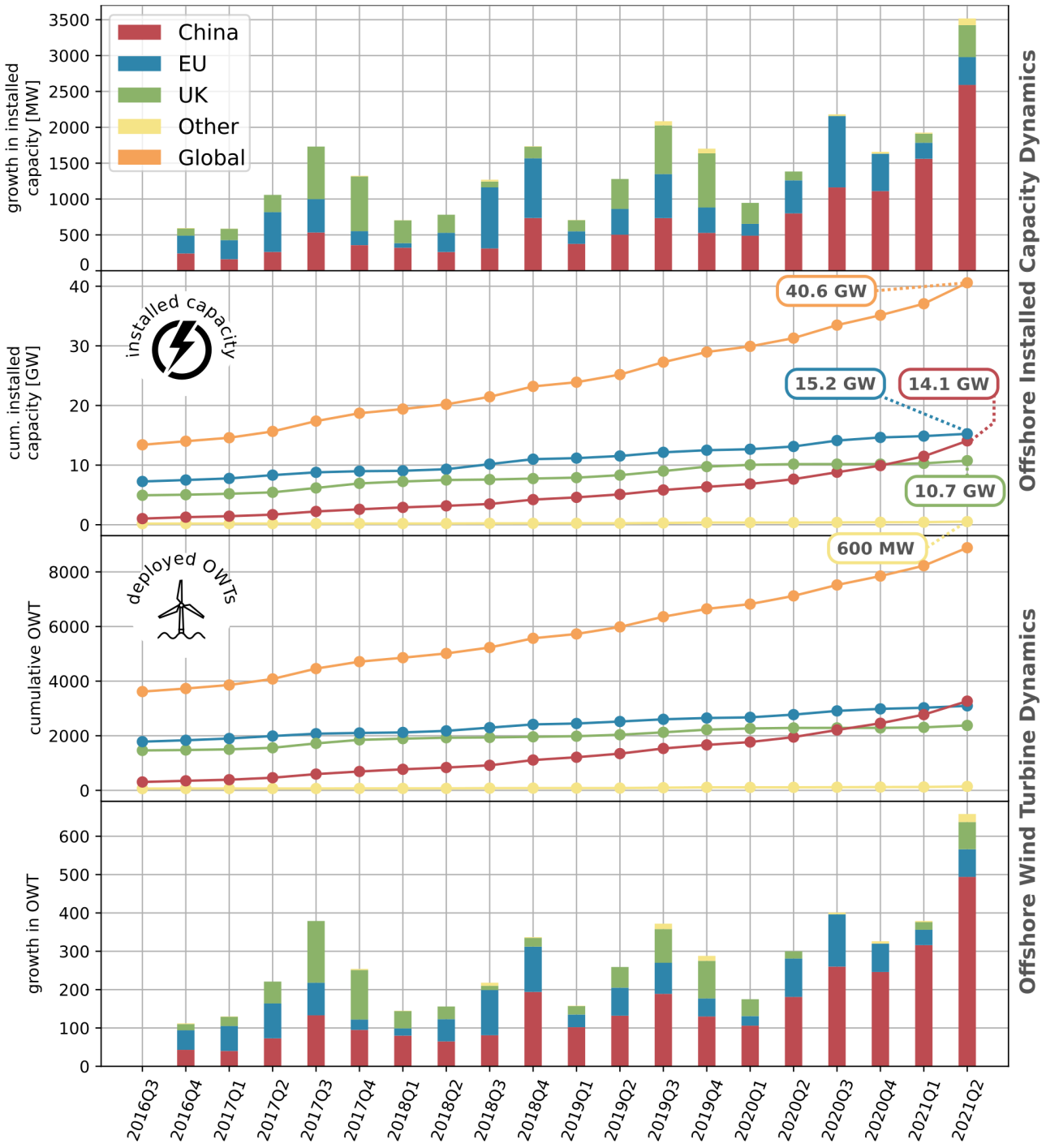

Figure 13. Temporal dynamics of the installed capacity (upper part) and the corresponding number of offshore wind turbines (lower part) aggregated by regions. The time series shows the quarterly evolution for five years between July 2016 and June 2021.

jacket foundations, which are fixated by using caissons or; gravity foundations, which stand directly on the seabed. All of them are used in water depths up to 50 m, as reported in the last row of figure 16. Regional differences can clearly be observed between China, the EU and UK. Large parts of the recently built OWTs in China are in nearshore areas with

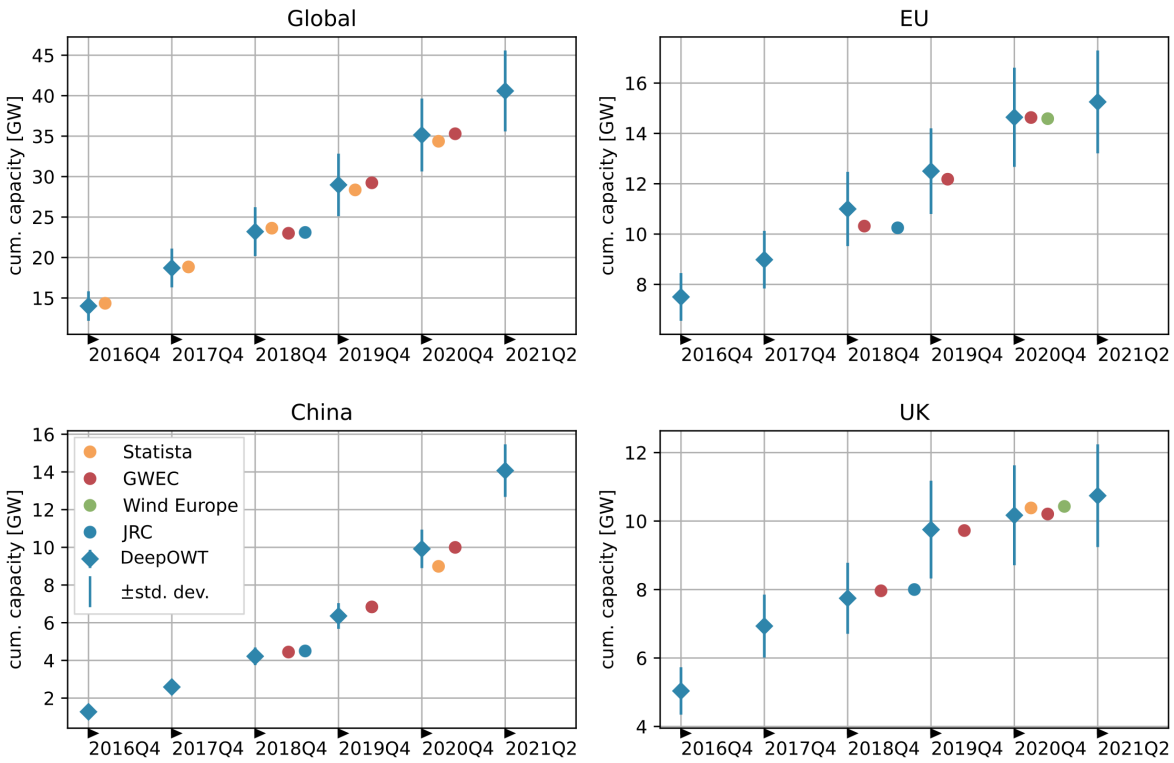

Figure 14. Validation of the estimated installed capacity, aggregated by larger regions and countries based on the DeepOWT data set compared to official reports by multiple institutions: Statista [24,25] , Global Wind Energy Council (GWEC) [16,17], Wind Europe [21] and European Commission Joint Research Centre (JRC) [7].

a strong tidal influence and therewith shallow water depth. Even when these areas can also be found in the coastal environments of the EU and UK, they are not used for OWT deployment, primarily due to strict nature reserve regulations of tidal flats.

In addition to these general observations regarding water depth, several outliers stand out, both from the temporal and regional perspectives. These outliers do not come from wrong bathymetry estimates of the underlying ETOPO1 data set but are pilot projects of floating offshore wind farms that allow offshore wind turbines to be installed in deeper water depths and with less construction-related impact on the seabed. In 2017 UK's Hywind Scotland swimming wind farm was installed in the North Sea Basin, followed by the WindFloat project at the Portuguese Atlantic coast in the EU in 2020, see figure 17. These two pilot projects are of major interest since they proved that floating offshore wind farms are technically feasible, and by continuing maturity of this technique and larger project sizes will also become acceptable from an economic perspective [2]. Floating wind farms will play a major role for the EU since they increase the number of possible offshore wind farms deployment sites. This is especially important for the Atlantic and Mediterranean coasts with typically steeply sloping water depths compared to the North Sea Basin and Baltic Sea. Figure 17 provides an overview of the European bathymetry with the water depth given for the two mentioned pilot projects as well as the median water depth of all OWTs in the EU. With the development of new technologies for the offshore wind industry, the EU and UK continue in their role as pioneers in this technology.

6. Discussion

In this study, freely available Earth observation and GIS data were used to generate a database, which can provide in-depth information about the development of the offshore wind energy sector on multiple temporal and spatial scales. The comparison with third-party surveys, especially the established reports of the Global Wind Energy Council [16, 17] and Wind Europe [21] demonstrate that the proposed approach can be used to provide detailed insights into the spatiotemporal evolution of the offshore wind energy sector. The OWT analysis delineates the offshore wind energy sector in a transition phase between decades of reaching maturity and at the beginning of a global expansion of large-scale offshore wind energy production. In addition to that, the still ongoing development of new technologies, like

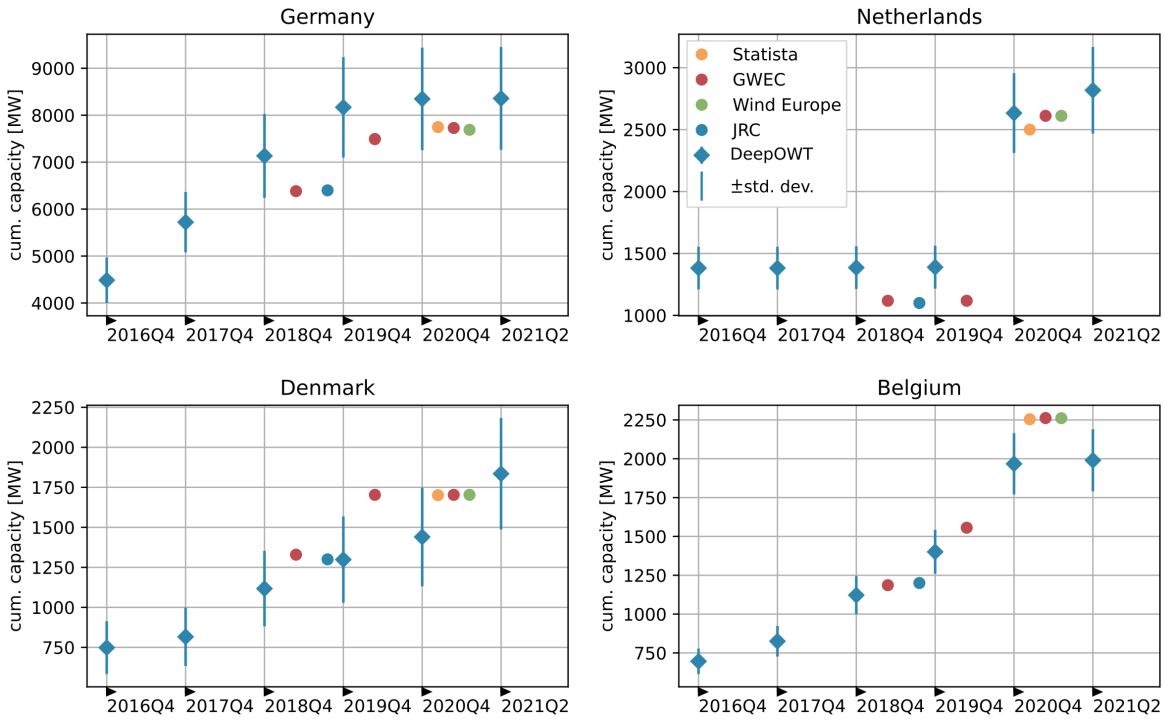

Figure 15. Validation of the estimated installed capacity, aggregated by the largest offshore wind energy producing EU members based on the DeepOWT data set compared to official reports by multiple institutions: Statista [24, 25] , Global Wind Energy Council (GWEC) [16, 17], Wind Europe [21] and European Commission Joint Research Centre (JRC) [7].

floating wind turbines [2], open up future application areas of offshore wind farms [27]. This will lead to a further increase in offshore wind projects in the long term.

The proposed methods, especially for calculating OWT height and installed capacity, add important context to the recently proposed DeepOWT data set [13]. The results presented in this study provide insights into technical metrics commonly used to report about developments in the offshore wind energy sector [7, 16, 17, 21]. In order to provide more insights into the offshore wind energy sector, the data set has to be further discussed and contextualised by adding expert knowledge from outside the Earth observation and geoinformation domain. With its quarterly frequency, multiple aspects and their spatiotemporal influence on the offshore wind energy sector can be investigated, like the entry into force of legal decisions, new regulations on multi-use policies and nature reserve, price developments in the energy and CO2 markets, or subsidies for renewable energy [5]. Furthermore, the effects of offshore wind infrastructure on marine ecosystems can be investigated more easily when accurate spatiotemporal information is available, especially when their characteristic attributes can be derived from freely available data. With the upcoming growth of the offshore wind energy sector [22], these studies are of major importance to ensure that all stakeholders are getting involved [11], and negative effects are kept to a minimum during a phase of maximising installed capacities in marine and coastal ecosystems. For decision and policymakers who lead the dialogues between all stakeholders, it is possible to aggregate data in space and time flexibly to provide a quick overview and compare regions with each other.

Future analysis of Earth observation data can build on the proposed workflow and further improve the modelling of installed capacity. Technological improvements will become increasingly important than the hub height alone in order to maximise installed capacity. Thus, multiple variables will become necessary to estimate the installed capacity in the future. Primarily attributes provided in this study, such as the date of deployment and minimum distance to the nearest neighbour, can be used potentially. The deployment date is suitable to communicate technological improvements gained over time. The minimum distance among OWTs is indirectly related to the rotor diameter, a crucial metric to investigate the installed capacity. Thus, refining the approach to estimating the installed capacity is a future task to consolidate global monitoring of the offshore wind energy sector with Earth observation data.

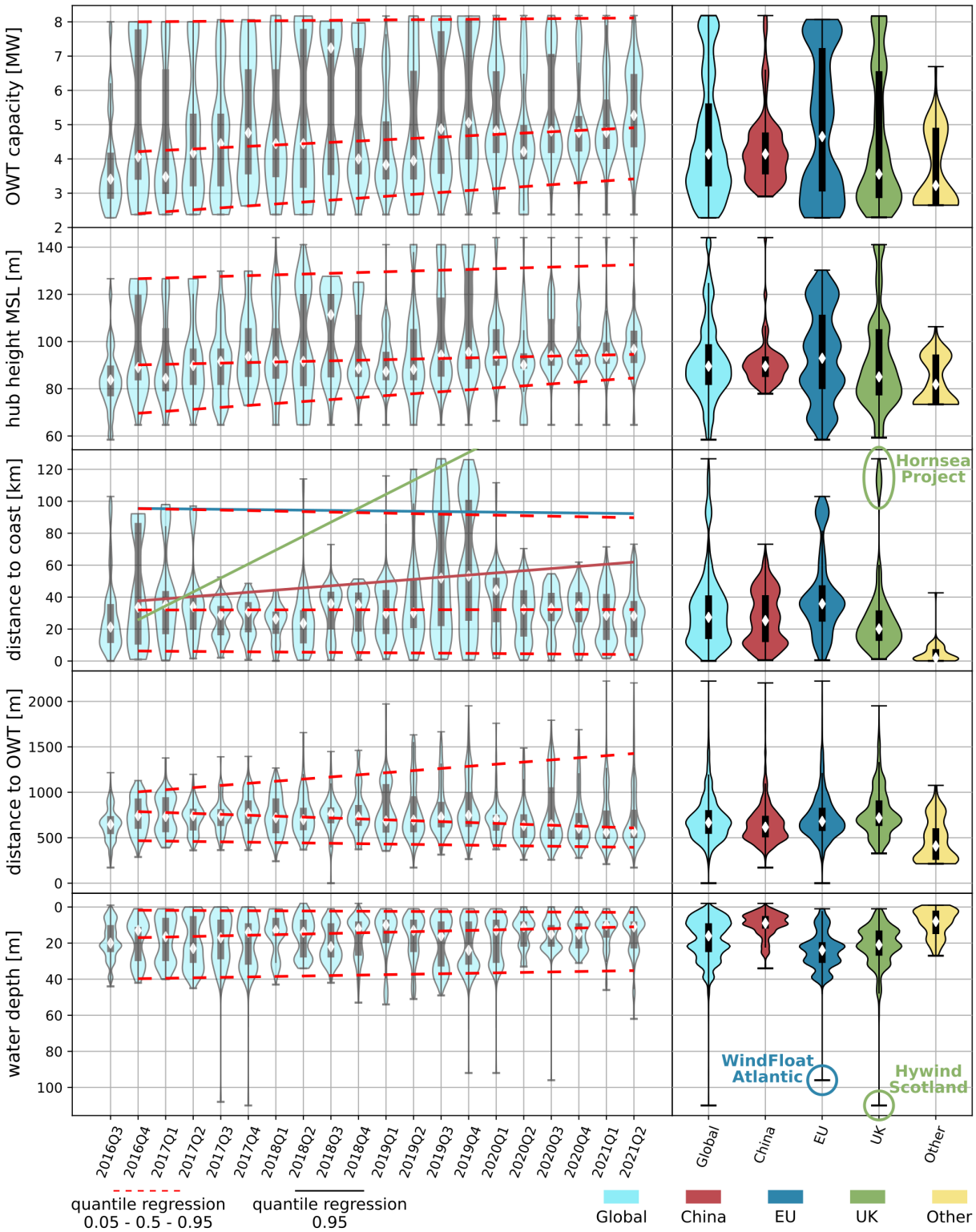

Figure 16. On the left side are the temporal dynamics between July 2016 and June 2021 of the offshore wind turbine (OWT) related attributes on a global scale. The dashed trend lines show the 0.05-0.5-0.95 quantile regressions. For the attribute distance to coast, the 0.95 quantile regression for the regions EU, UK and China are provided separately. On the right side, the same attributes are aggregated by regions for the entire period.

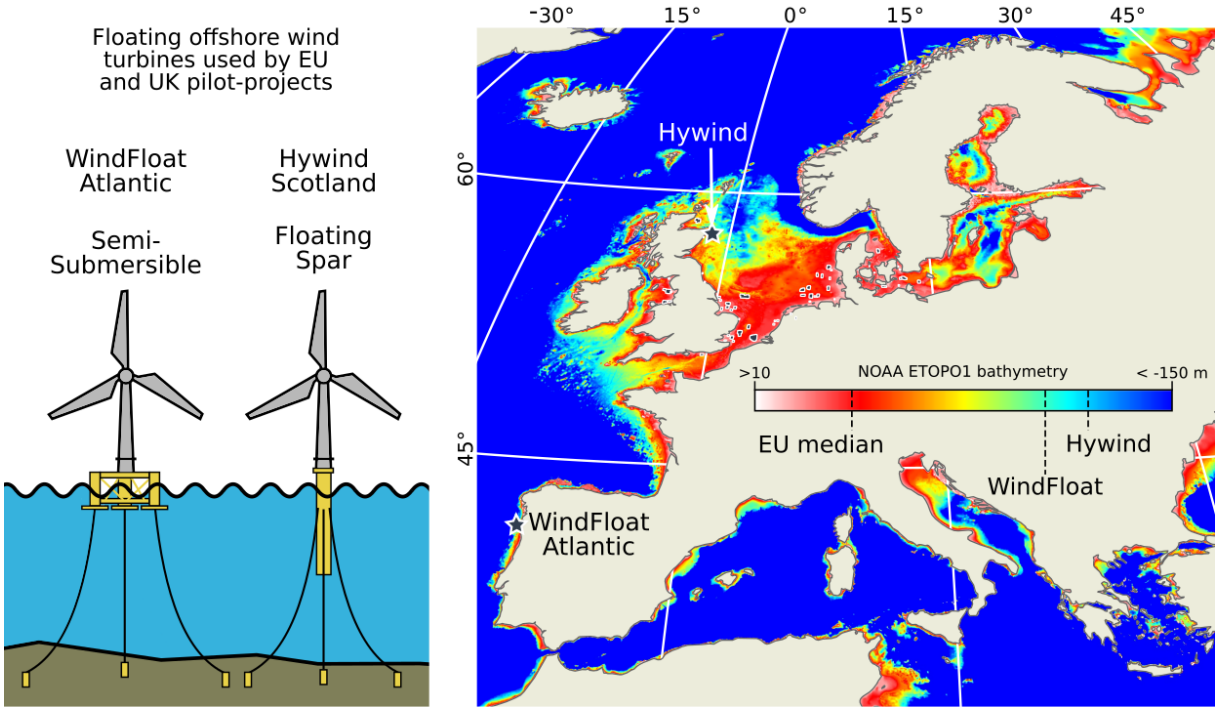

Figure 17. Two types of floating wind turbines and their usage in two EU pilot projects. Next to it, the bathymetry of the EU and UK, along with the locations of the two swimming offshore wind farm projects Hywind in Scotland and WindFloat at the Portuguese coast. The EU median label on the colour ramp indicates the median water depth of all OWF's in the EU.

7. Conclusion

This study analysed the installed capacity of offshore wind turbines (OWT) globally, along with further attributes frequently used to report on developments in the offshore wind energy sector. Thereby the analysis is based on freely available Earth observation and GIS data. Mainly, the recently proposed global data set of OWT, the DeepOWT data set [13], and the Sentinel-1 archive were investigated.

Between July 2016 and June 2021 additional 5,268 OWTs with a derived cumulative capacity of 27.2 GW were deployed worldwide. The cumulative installed capacity in June 2021 was 40.6 GW provided by 8,885 OWTs. Thus within the investigated five years, the installed capacity was increased by 200%. The three major contributors are the European Union (EU) (3,096 OWTs and 15.2 GW), China (3,267 OWTs and 14.1 GW), and the United Kingdom (UK) (2,378 OWTs and 10.7 GW). China had the highest growth rate with 13 GW and 2,960 OWTs. In the same period, the offshore wind sector in the EU and UK grew by 8 GW and 1,313 OWTs, and 5.8 GW and 916 OWTs, respectively. Most OWTs were deployed and are still under construction in the North Sea Basin and the East and the South China Sea. With new technologies like floating wind farms, water depths deeper as 50 m will become accessible in future. The deepest depth of 110 m is of the European pilot project Hywind Scotland.

A progressively larger distance between recently deployed OWTs and the shoreline indicates that at established regions of wind energy production, potential offshore areas close to the coast have already been exploited. This aspect and the high number of recently constructed artificial objects in marine ecosystems make it obvious that integrated planning that includes all stakeholders involved in coastal and marine space is necessary. Future research that further investigates the proposed methods and data is necessary to add expert knowledge from other domains to ensure that carbon-neutral energy production with offshore wind turbines is as sustainable as possible.

Acknowledgements

The authors would like to thank ESA's Copernicus program for providing free access to the Sentinel-1 data and the Google Earth Engine platform for preprocessing and making the data accessible. We would like to thank Achim Roth for a fruitful conversation about the radargrammetric interpretation.

Funding

This research received no external funding.

Declaration of competing interest

The authors declare no conflict of interest.

Author Contributions

TH designed the study, collected the ground truth data, developed and implemented the code for data processing, visualisation and evaluation, and prepared the original manuscript, including figures. CK supervised the study, gave suggestions for figures and repeatedly commented and discussed the manuscript.

References

[1] C. Amante and B. W. Eakins. Etopo1 1 arc-minute global relief model: Procedures, data sources and analysis. noaa technical memorandum nesdis ngdc-24, 2009. 4, 11

[2] R. Chitteth Ramachandran, C. Desmond, F. Judge, J.-J. Serraris, and J. Murphy. Floating offshore wind turbines: Installation, operation, maintenance and decommissioning challenges and opportunities [preprint]. *Wind Energy Science Discussions*, 2021:1–32, 2021. 15, 16

[3] COP26. Global coal to clean power transition statement. https://ukcop26.org/global-coal-to-clean-power-transition-statement/. last visited 07.01.2022, 2021. 2

[4] COP26. Zero emission vehicles transition council: 2022 action plan. https://ukcop26.org/zero-emission-vehicles-transition-council-2022-action-plan/. last visited 07.01.2022, 2021. 2

[5] M. deCastro, S. Salvador, M. Gómez-Gesteira, X. Costoya, D. Carvalho, F.J. Sanz-Larruga, and L. Gimeno. Europe, china and the united states: Three different approaches to the development of offshore wind energy. *Renewable and Sustainable Energy Reviews*, 109:55–70, 2019. 16

[6] European Commission. An eu strategy to harness the potential of offshore renewable energy for a climate neutral future. https://ec.europa.eu/energy/sites/ener/files/offshore_renewable_energy_strategy.pdf. last visited 10.06.2021, 2020. 2, 11

[7] European Commission, Joint Research Centre, C Vazquez Hernandez, and T Telsnig. *Wind energy : technology market report*. Publications Office, 2019. 15, 16

[8] Flanders Marine Institute. Union of the esri country shapefile and the exclusive economic zones (version 3). https://www.marineregions.org/. last visited 10.02.2022, 2020. 4, 11

[9] Noel Gorelick, Matt Hancher, Mike Dixon, Simon Ilyushchenko, David Thau, and Rebecca Moore. Google earth engine: Planetary-scale geospatial analysis for everyone. *Remote Sensing of Environment*, 202:18–27, 2017. Big Remotely Sensed Data: tools, applications and experiences. 4

[10] Laura Florentina Gusatu, Claudia Yamu, Christian Zuidema, and André Faaij. A spatial analysis of the potentials for offshore wind farm locations in the north sea region: Challenges and opportunities. *ISPRS International Journal of Geo-Information*, 9(2):96, 2020. 2

[11] L. Gușatu, Stefano Menegon, D. Depellegrin, C. Zuidema, A. Faaij, and Claudia Yamu. Spatial and temporal analysis of cumulative environmental effects of offshore wind farms in the north sea basin. *Scientific Reports*, 11, 2021. 16

[12] Thorsten Hoeser, Felix Bachofer, and Claudia Kuenzer. Object detection and image segmentation with deep learning on earth observation data: A review—part ii: Applications. *Remote Sensing*, 12(18), 2020. 2

[13] T. Hoeser, S. Feuerstein, and C. Kuenzer. Deepowt: A global offshore wind turbine data set derived with deep learning from sentinel-1 data. *Earth System Science Data Discussions*, 2022:1–26, 2022. 2, 3, 4, 16, 18

[14] Thorsten Hoeser and Claudia Kuenzer. Object detection and image segmentation with deep learning on earth observation data: A review-part i: Evolution and recent trends. *Remote Sensing*, 12(10), 2020. 2

[15] Thorsten Hoeser and Claudia Kuenzer. Synteo: Synthetic dataset generation for earth observation with deep learning - demonstrated for offshore wind farm detection. *CoRR*, abs/2112.02829v2, 2021. 4

[16] Joyce Lee and Feng Zhao. *GWEC - Global Wind Report 2019*. Global Wind Energy Council, 2020. 15, 16

[17] Joyce Lee and Feng Zhao. *GWEC - Global Wind Report 2021*. Global Wind Energy Council, 2021. 15, 16

[18] Lei Ma, Yu Liu, Xueliang Zhang, Yuanxin Ye, Gaofei Yin, and Brian Alan Johnson. Deep learning in remote sensing applications: A meta-analysis and review. *ISPRS Journal of Photogrammetry and Remote Sensing*, 152:166 – 177, 2019. 2

[19] Stephane Meric, Franck Fayard, and Eric Pottier. Radargrammetric sar image processing. In Pei-Gee Peter Ho, editor, *Geoscience and Remote Sensing*, chapter 20. IntechOpen, Rijeka, 2009. 4

[20] Natural Earth. 1:10m physical vectors. https://www.naturalearthdata.com/downloads/10m-physical-vectors/. last visited 10.02.2022, 2022. 4, 8

[21] Lizet Ramírez, Daniel Fraile, Guy Brindley, Rory O'Sullivan, Laia Miró, and Lin Van de Velde. *Offshore Wind in Europe - Key trends and statistics 2020*. Wind Europe, 2021. 15, 16

[22] S. Rodrigues, C. Restrepo, E. Kontos, R. Teixeira Pinto, and P. Bauer. Trends of offshore wind projects. *Renewable and Sustainable Energy Reviews*, 49:1114–1135, 2015. 2, 11, 16

[23] Nikolai V Smirnov. Estimate of deviation between empirical distribution functions in two independent samples. *Bulletin Moscow University*, 2(2):3–16, 1939. 7

[24] Statista. Global offshore wind energy capacity from 2009 to 2020. https://www.statista.com/statistics/476327/global-capacity-of-offshore-wind-energy/. last visited 10.02.2022, 2021. 15, 16

[25] Statista. Wichtigste länder weltweit nach installierter offshore-windenergieleistung im jahr 2020. https://de.statista.com/statistik/daten/studie/158501/umfrage/kapazitaeten-der-offshore-windkraft-nach-laendern-im-jahr-2009/. last visited 10.02.2022, 2021. 15, 16

[26] Ramon Torres, Paul Snoeij, Dirk Geudtner, David Bibby, Malcolm Davidson, Evert Attema, Pierre Potin, BjÖrn Rommen, Nicolas Floury, Mike Brown, Ignacio Navas Traver, Patrick Deghaye, Berthyl Duesmann, Betlem Rosich, Nuno Miranda, Claudio Bruno, Michelangelo L'Abbate, Renato Croci, Andrea Pietropaolo, Markus Huchler, and Friedhelm Rostan. Gmes sentinel-1 mission. *Remote Sensing of Environment*, 120:9–24, 2012. The Sentinel Missions - New Opportunities for Science. 4, 5

[27] UK Gov. *Net Zero Strategy: Build Back Greener*. HM Government, London, 2021. 2, 11, 16

[28] Brian A. Wong, Christian Thomas, and Patrick Halpin. Automating offshore infrastructure extractions using synthetic aperture radar and Google Earth Engine. *Remote Sensing of Environment*, 233:111412, 2019. 3

[29] Wenxuan Xu, Yongxue Liu, Wei Wu, Yanzhu Dong, Wanyun Lu, Yongchao Liu, Bingxue Zhao, Huiting Li, and Renfei Yang. Proliferation of offshore wind farms in the north sea and surrounding waters revealed by satellite image time series. *Renewable and Sustainable Energy Reviews*, 133:110167, 2020. 4

[30] Ting Zhang, Bo Tian, Dhritiraj Sengupta, Lei Zhang, and Yail Si. Global offshore wind turbine dataset. *Scientific Data*, 8(191), 2021. 4

[31] X. X. Zhu, D. Tuia, L. Mou, G. Xia, L. Zhang, F. Xu, and F. Fraundorfer. Deep learning in remote sensing: A comprehensive review and list of resources. *IEEE Geoscience and Remote Sensing Magazine*, 5(4):8–36, 2017. 2